Journal of Organometallic Chemistry 694 (2009) 3958–3964

Contents lists available at ScienceDirect

Journal of Organometallic Chemistry

journal homepage: www.elsevier.com/locate/jorganchem

Novel ferrocenyl nitroxides: Synthesis, structures, electrochemistry and antioxidative activity

Xiao Qiu, Hongli Zhao, Minbo Lan *

Key Laboratory for Advanced Materials and Research Centre of Analysis Test, East China University of Science and Technology, Shanghai 200237, PR China

ARTICLE INFO

Article history:
Received 25 May 2009
Received in revised form 7 August 2009
Accepted 10 August 2009
Available online 14 August 2009

Keywords:
Ferrocenyl nitroxides
X-ray structure
Antioxidative activity
Electrochemistry

ABSTRACT

Novel ferrocenyl nitroxides **3**–**6** were prepared as models for studying the linkage structure–activity relationship. Single-crystal X-ray structures of compounds **4** and **5** were determined and comparatively studied. The *in vitro* antioxidative activities (e.g. scavenging superoxide anion and hydroxide radical) of compounds **3**–**6** and 4-ferrocenamido-2,2,6,6-tetramethyl-piperidin-oxy (**2**) were evaluated. Compounds **3** and **5** exhibit high scavenging activities in low concentration. Results from electrochemistry and UV/Vis spectroscopy show that the redox property and antioxidative activity are closely related to the structure of the linkage bridging ferrocene and cyclic nitroxide moieties. The results further indicate that the ferrocene moiety plays a principal role in antioxidation. The modification of linkage was found to be able to decrease the ferrocene/ferrocenium potential and improve the antioxidative activity effectively.

1. Instruction

Since the first member (*t*-butylferrocenylnitroxide) was reported at 1969 [1], the family of metallocenyl substituted nitroxide radical (McNO) became an important kind of compounds in the interdisciplinary field between organometallic and free radical field [2–4]. Most McNOs research had focused on discussing the intermolecular ferromagnetic interaction, and aimed at the preparation of high-spin materials [5,6], but other potential properties and application of McNOs have been extensively overlooked. In recent years, during our work of employing new McNOs as *in vivo* electron paramagnetic resonance (EPR) oximetry probes, we surprisingly found these compounds not only keep the parent compounds' nature, e.g. high-spin magnetic property, redox activity and exceptional stability, but also exhibit improved functionalities. We recently reported the relationship between the antioxidative ability and the anticancer activity of some McNOs (e.g. **1** and **2**, Scheme 1) [7–9].

It is possible that molecular design and synthesis will yield new superior McNOs with excellent properties, which will be widely used in various biological and pathological areas as spin labels, EPR oximetry probes, antioxidants and anticancer drugs. The present McNO molecular design and synthesis have been just confined to introducing different nitroxide moiety into different metallocenyl ring directly or by a short linkage [2,6,7]. However, using various longer conjunctional linkage bridging the metallocene and the nitroxide moieties, could be an even better choice with many alternatives, which has been less reported, presumably because of the ambiguity of the relationship between linkage structure and compounds properties. So in the development of novel functional McNOs, two fundamental issues must be addressed, (1) whether the longer and more complex linkage improves the McNO properties? (2) and how does it improve these properties?

In this paper, we designed and prepared a family of novel McNOs as research models, and addressed such above described issues by comparing their single-crystal X-ray structures, *in vitro* antioxidative activities, electrochemical properties and UV/Vis spectra. This work not only preliminarily explored the relationship between linkage structure and the electrochemical nature, as well as the biological activity of compounds, but also would guide us in formulating a strategy of designing and synthesizing new functional McNOs with preferable biological activities such as antioxidative ability, radiation protection, DNA protection and anticancer activity.

2. Results and discussion

2.1. Synthesis

The studied compounds **3**–**6** (Scheme 2) were synthesised by coupling ferrocenyl carboxylic acids with 4-amino-2,2,6,6-tetramethyl-piperidin-oxyl (4-amino-TEMPO) radical. The ferrocenyl acetic acid was prepared from acetylferrocene via Willgerodt–Kindler reaction [10,11]. The *trans*-ferrocenylacrylic acid was synthesised by formylferrocene decarboxylative Knoevennagel

* Corresponding author. Tel.: +86 21 64253574; fax: +86 21 64252947.
E-mail address: minbolan@ecust.edu.cn (M. Lan).

0022-328X/$ - see front matter © 2009 Elsevier B.V. All rights reserved.
doi:10.1016/j.jorganchem.2009.08.012

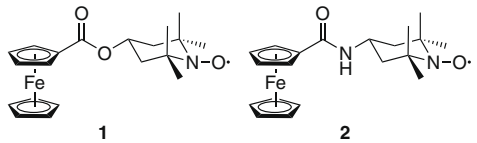

1 2

Scheme 1.

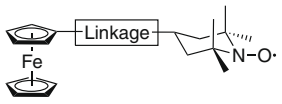

Linkage **3**: –CH_2CONH–
4: –CH=CHCONH–
5: –CH_2CH_2CONH–
6: –$COCH_2CH_2CONH$–

Scheme 2.

condenation with malonic acid [12]. Then *trans*-ferrocenylacrylic acid was further catalytic hydrogenated into β-ferrocenyl-propionic acid [13,14]. The β-ferrocenoylpropionic acid was obtained by the Friedel-Crafts acylation of ferrocene with succinic anhydride [15]. The condensation of these ferrocenyl carboxylic acids with 4-amino-TEMPO radical in the presence of 1,3-dicyclohexylcarbodiimide (DCC) and 1-hydroxylbenzotriazole (HOBt) as catalysts yielded the corresponding amides **3**–**6** [16]. The purification was performed by silica-gel column chromatography using the solvent system of petroleum ether(60–90 °C)/ethyl acetate as eluent to afford **3**–**6** as yellow or red prisms (yield: 54–76%).

2.2. Structure analysis of *4* and *5*

Among all four compounds, compounds **4** and **5** are very similar in chemical structure. The only structural difference between them is the C=C bond in **4** being replaced by C–C bond in **5**. Hence it is interesting and meaningful to compare their single crystal structures to research the double/single-bond effect on their geometry.

The X-ray diffraction analysis of compound **4** reveals two crystallographically independent molecular conformations (**4a** and **4b**, Fig. 1). The selected bond lengths and angles of **4a** and **4b** are given in the caption of Fig. 1. Conformations **4a** and **4b** are geometrically identical. The key difference between the two conformations is the degree of rotation around the bond between the substituted cyclopentadienyl (Cp_{sub}) ring and C=C–C=O plane. In **4a**, the torsion angles of C9=C10–C11=C12 and C11=C12–C13=O1 are −11.6(11)° and −1.3(9)°, and the dihedral angle of acryl and Cp_{sub} is −13.71°, which indicated that the C=C–C=O is planar and approximately coplanar with the Cp_{sub} ring. The bond lengths of C10–C11 (1.449(8) Å), C11–C12 (1.329(8) Å) and C12–C13 (1.487(8) Å) are intermediate between single and double bonds. These values point to an extended π electron conjugated system over the acryl and the Cp_{sub} ring, similar to that found in vinyl ferrocene [17].

In **4b** the torsion angles of C9=C10–C11=C12 and C11=C12–C13=O1 are 22.48(14)° and 7.0(19)°, and the dihedral angle of C=C–C=O and Cp_{sub} is 26.65°, which are considerably larger than those in **4a**. The significant geometric difference can be rationalized by the existence of intermolecular hydrogen bond between carboxylic oxygen and N–H proton of adjacent **4b** molecules (Fig. 2), which forces the C=C–C=O to twist. The bond length of C11–C12 (1.270(11) Å) is a typical double bond length and shorter than the corresponding bond length in **4a**. The bond lengths of C10–C11 (1.460(11) Å) and C12–C13 (1.606(12) Å) are longer than the corresponding bond lengths in **4a**. The results clearly indicate

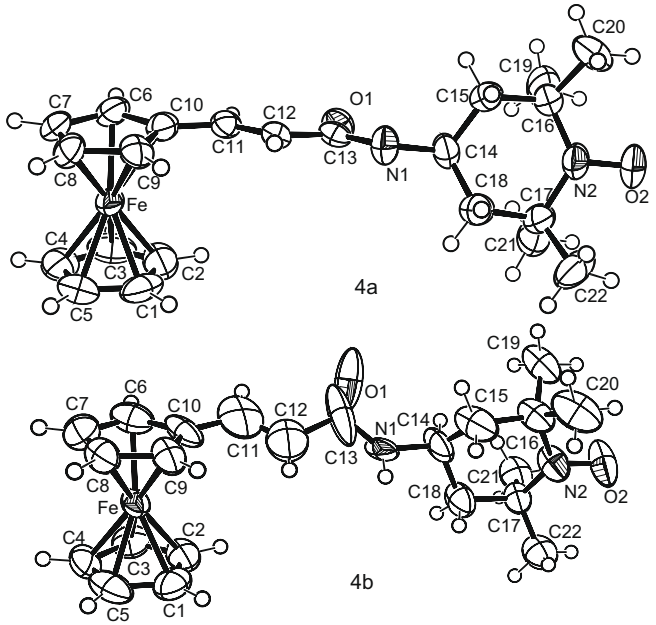

Fig. 1. OPTEP plots of the two conformations (**4a** and **4b**) of compound **4** in the crystal. Ellipsoids are given at a 50% probability level. Selected bond lengths [Å] and torsion angles [°]: **4a** C10–C11 1.449(8), C11–C12 1.329(8), C12–C13 1.487(8), C9–C10–C11–C12 – 11.6(11), C11–C12–C13–O1 – 1.3(9), C14–C15–C16–N2 – 47.8(8), N2–C17–C18–C14 46.5(8), C16–N2–C17–C18 – 37.6(9), C17–N2–C16–C15 38.3(9), C18–C14–C15–C16 60.0(8), O2–N2–C17–C18 165.3(6), O2–N2–C16–C15 – 164.7(6); **4b** C10–C11 1.460(11), C11–C12 1.270(11), C12–C13 1.606(12), C9–C10–C11–C12 22.4(14), C11–C12–C13–O1 7.0(19), C14–C15–C16–N2 – 44.1(10), N2–C17–C18–C14 43.2(9), C16–N2–C17–C18 – 27.8(9), C17–N2–C16–C15 28.3(10), C18–C14–C15–C16 61.5(9), O2–N2–C17–C18 173.3(7), O2–N2–C16–C15 – 172.8(7).

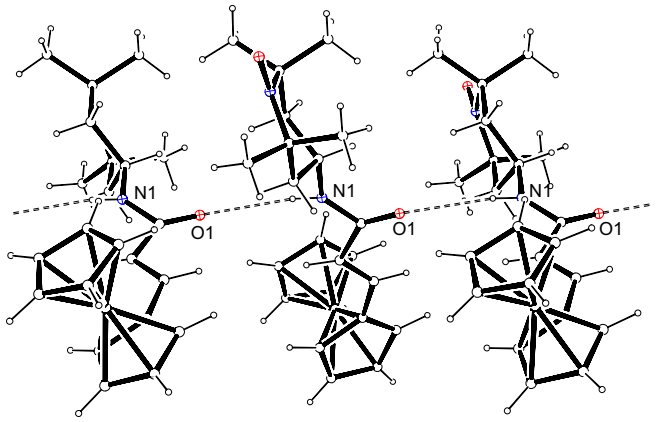

Fig. 2. Hydrogen bonding interactions between molecules **4b**.

that the extended π-electron conjugated system is broken by the torsion of the Cp_{sub} ring and C=C–C=O plane.

The crystal structure of compound **5** is depicted in Fig. 3. The selected bond lengths and angles of **5** are given in the caption of Fig. 3. The most relevant conformational feature of the compound **5** is that the ferrocenyl pendant is not lying on the Cp_{sub} plane, as would normally be expected for mono substituted metallocenyl bearing a linear substituent [13], but roughly perpendicular to the Cp_{sub} plane. The C9–C10–C11–C12 torsion angle is as large as 91.6(3)°.

An interesting finding is that the Fc moiety conformations of **5** and **4b** are more in agreement with that of ferrocene than that of **4a**. In **4b** and **5**, Fe atom is almost equidistant from the centroid

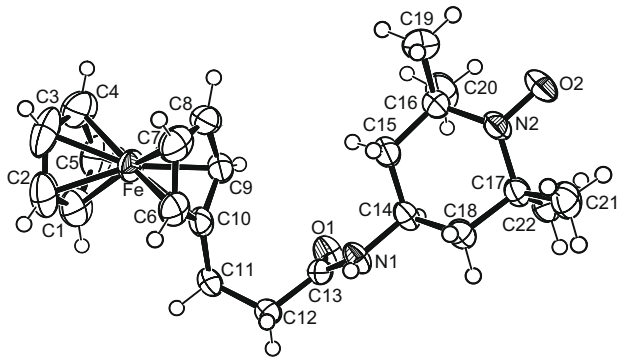

Fig. 3. ORTEP plot of compound **5** in the crystal. Ellipsoid is given at a 50% probability level. Selected bond lengths [Å] and torsion angles [°]: C9–C10–C11–C12 91.5(3), C11–C12–C13–O1 – 56.2(3), C14–C15–C16–N2 – 43.1(3), N2–C17–C18–C14 44.5(3), C16–N2–C17–C18 – 30.7(3), C17–N2–C16–C15 29.9(3), C18–C14–C15–C16 – 60.4(3), O2–N2–C17–C18 171.1(2), O2–N2–C16–C15 – 172.0(2).

of the Cp_{sub} and the centroid of the unsubstituted cyclopentadienyl (Cp_{unsub}), the distances of Fe–Cp_{sub}/Fe–Cp_{unsub} are **4b** 1.643(13)/1.641(13) Å and **5** 1.643(29)/1.645(29) Å; while in **4a**, the Fe atom is closer to the Cp_{sub} ring, the distances of Fe–Cp_{sub}/Fe–Cp_{unsub} are 1.636(28)/1.651(29) Å. The Cp rings of **4b** and **5** are more nearly parallel and eclipsed compared to **4a**. The tilt angles are **4a** 2.18°, **4b** 1.18° and **5** 1.36° from the parallelism. And the twist angles are **4a** 5.87°, **4b** 3.26° and **5** 0.26° from the eclipsed conformation. On the other hand, although the conformations of the TEMPO rings of **4a**, **4b** and **5** are all shallow chair form, the ring conformation of **4b** is more similar to **5** than to **4a**. The torsion angles within the TEMPO rings of **4b** and **5** are C–C–C–N2 (C14–C15–C16–N2, C14–C18–C17–N2) ±43.1(2)° to ±44.5(3)°, C–N2–C–C (C16–N2–C17–C18, C17–N2–C16–C15) ±27.8(9)° to ±30.7(3)°, O2–N2–C–C (O2–N2–C16–C15, O2–N2–C17–C18) ±171.1(2)° to ±173.3(7)°, while the torsion angles within the ring of **4a** are C–C–C–N2 ±46.5(8)° to ±47.5(8)°, C–N2–C–C ±37.6(9)° to ±38.3(9)°, O2–N2–C–C ±164.7(6)° to 165.3(6)°. The results indicate that extended conjugated system obviously has influence on the geometry of the Fc and TEMPO skeletons; however, when the extended conjugated system is broken, this influence disappears.

2.3. Antioxidative activity

Reactive oxygen species (ROS) like the superoxide radical anion ($O_2^{\cdot-}$) and hydroxyl radical (·OH) generated in biological system, can oxidatively damage biomolecules such as DNA, protein, lipids, cell membrane etc., initiating cancer and cardiovascular diseases [18,19]. So one goal of our lab is to develop effective antioxidants. Because cyclic nitroxides, e.g. 4-amino-TEMPO and 4-hydroxyl-TEMPO, have been recognized as a class of antioxidant compounds for a long time, and some ferrocene derivatives have been also reported as antioxidants [20,21], we speculated that these compounds (**3**–**6**) containing TEMPO and ferrocene subunits could exhibit improved antioxidative activities. To evaluate the *in vitro* antioxidative activity of materials, two of the most commonly used methods are UV/Vis method and chemiluminescence (CL) method. Because the result of UV/Vis method would be interfered by the precipitate formed in the assay process, we used CL method to measure antioxidative activities of compounds (**3**–**6**). The superoxide radical anion ($O_2^{\cdot-}$) scavenging activities were assayed by a pyrogallol-luminol system CL and the hydroxyl radical (·OH) scavenging activities were measured by $CuSO_4$–phenanthroline–ascorbate–H_2O_2 system CL [22–24]. For comparison, the compound **2** was also included in the experiments.

As shown in Figs. 4 and 5, the scavenging activities upon ($O_2^{\cdot-}$) and (·OH) rise with the increasing of the concentration of samples,

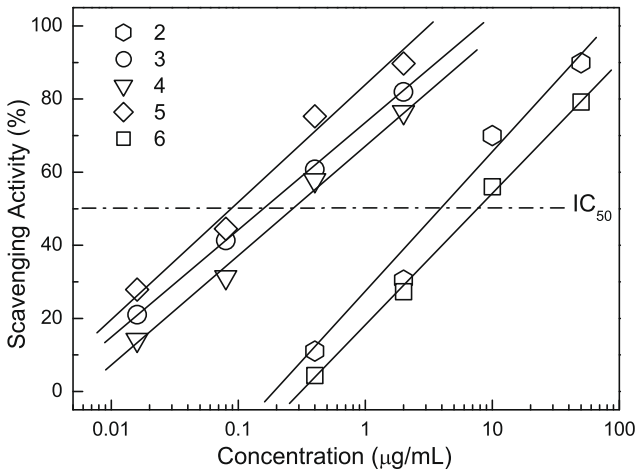

Fig. 4. Comparison of the $O_2^{\cdot-}$ scavenging activities of compounds **2**–**6** at various concentrations. Each point of the graph is the mean value of three separate assays.

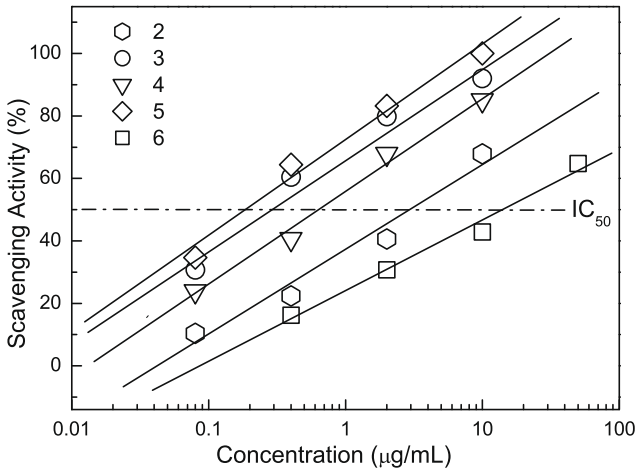

Fig. 5. Comparison of the (·OH) scavenging activities of compounds **2**–**6** at various concentrations. Each point of the graph is the mean value of three separate assays.

and linear relationships ($R^2 > 0.95$) between the base 10 logarithm of sample's concentration and inhibition rate could be established in a certain concentration range [25]. In order to compare the scavenging effects of various compounds, the concentration values of 50% inhibition (IC_{50}) were determined according to the linear relationship and summarized in Table 1.

Based on these IC_{50} results, the linkage structure–activity relationship was observed. Compounds **3**, **4** and **5**, without a carbonyl directly adjacent to Fc moiety, show high scavenging ROS activity in low concentration. Among them, compound **5** shows the highest ROS scavenging activity, followed by **3** with one less bond, and **4** with a double bond. The compound **2** and **6** with a carbonyl directly adjacent to the Fc moiety exhibit ROS scavenging activity

Table 1
$O_2^{\cdot-}$ and ·OH scavenging activity IC_{50} [μmol/L] of the compounds **2**–**6**.[a]

Com.p.	IC_{50} (scavenging $O_2^{\cdot-}$)	IC_{50} (scavenging ·OH)
2	11.8	8.02
3	0.42	0.66
4	0.66	1.57
5	0.22	0.47
6	17.7	32.5

[a] IC_{50} values were calculated by linear relationship ($R^2 > 0.95$).

at much higher concentration. The **6** containing double carbonyls exhibits lower scavenging activity compared to **2** with one carbonyl. Additionally, the five compounds show improved antioxidative activity compared to their parent compounds. For example, the scavenging $O_2^{\cdot -}$ activity of compound **2** is much higher than that of the ferrocenyl carboxylic acid (IC_{50} 0.98 mmol/L) reported before [26].

2.4. Electrochemistry and UV/Vis spectroscopy

Antioxidative activity is closely related to the redox property of materials. In order to further understand the relationship between the linkage structure and the antioxidative activity, compounds **2**–**6** were studied by electrochemistry and UV/Vis absorption spectroscopy. The cyclic voltammetry assays of **2**–**6** were carried out by a three-electrode system consisting of a platinum working electrode, a platinum wire counter electrode and a saturated calomel reference electrode (SCE) [27], at different sweep rates ranging from 0.02 to 0.80 Vs^{-1}. As shown in Fig. 6, all radicals show cyclic voltammograms (CVs) comprising two single-electron redox reactions between 0 and 1.0 V. These oxidation processes are found to be nearly reversible with peak potential separations $\Delta E_p(E_{pc}-E_{pa})$ of ⩽70 mV. From the CVs at different sweep rates, the dependences of the peak current (i_p) on the square root of the scan rate ($v^{1/2}$) are linear for all oxidation peaks, indicating that these electrochemistry processes are purely diffusion controlled [28]. For all the studied compounds, we assigned the first single-electron oxidation in the low-potential region for the oxidation of the Fc to ferrocenium (Fc^+) [29], and the second single-electron oxidation in the high-potential region for the oxidation nitroxide radical (TEMPO) to oxoammonium cation ($TEMPO^+$)(Scheme 3) [30,31]. Based on the half-wave potentials ($E_{1/2}$) determined by $(E_{pa}+E_{pc})/2$, the tendencies of Fc and TEMPO oxidation potentials were obtained as **5** < **3** < **4** < **2** < **6** and **6** < **5** < **3** < **2** < **4**, respectively (Table 2).

The UV/Vis spectra of compounds **2**–**6** were measured in CH_2Cl_2 solution between 300 and 600 nm. As shown in Fig. 7, the spectra of compounds **2**, **4** and **6** show two main absorption bands at λ_{max} 304–360 nm and λ_{max} 448–465 nm, attributed to π–π* transition

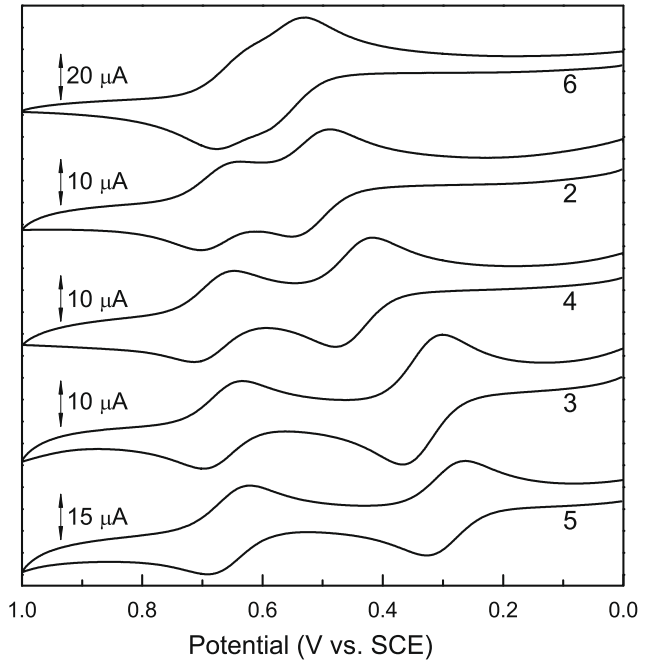

Fig. 6. Comparison of the CVs for **2**–**6** (0.5 mmol/L) in acetonitrile solution (0.1 mol/L $LiClO_4$) at platinum electrode, scan rate: 0.05 Vs^{-1}.

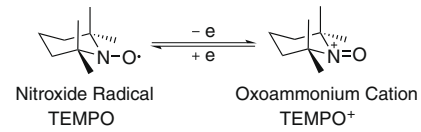

Scheme 3.

Table 2
Electrochemical parameters [V vs SCE] of **2**–**6**.[a]

Com.p.	E_{pa}^1	E_{pc}^1	ΔE_p^1	$E_{1/2}^1$	E_{pa}^2	E_{pc}^2	ΔE_p^2	$E_{1/2}^2$
2	0.551	0.488	0.063	0.519	0.702	0.636	0.065	0.669
3	0.369	0.300	0.069	0.334	0.698	0.633	0.065	0.665
4	0.478	0.416	0.062	0.447	0.715	0.647	0.068	0.681
5	0.326	0.263	0.063	0.295	0.690	0.621	0.070	0.655
6	0.587	0.529	0.058	0.558	0.675	0.611	0.064	0.643

[a] Measured by voltammetry assays; E_{pa}: anodic peak potential; E_{pc}: cathodic peak potentials; $\Delta E_p = E_{pc}-E_{pa}$; $E_{1/2} = (E_{pc}+E_{pa})/2$.

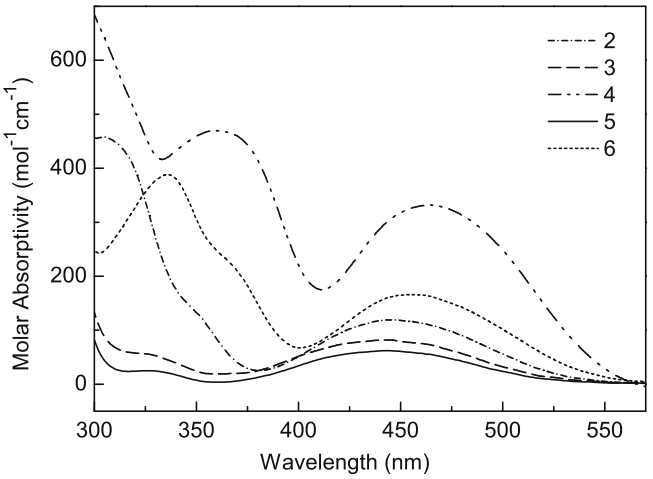

Fig. 7. The UV/Vis spectra of **2**–**6** (1 mmol/L) in CH_2Cl_2 solution.

and the forbidden *d*–*d* transition located on Fc moiety, respectively [32], while the spectra of **3** and **5** only show the *d*–*d* transition band at λ_{max} 442–444 nm with much lower intensity. The bathochromic shifts of absorption maxima of **2**, **4** and **6** relative to **3** and **5** are evidence of the existence of extended conjugated system upon the linkages and the Fc moieties in **2**, **4** and **6**. The electron delocalization in the conjugated system not only makes the electron transition easier, but also decreases the electron density of Fc and makes it harder to be oxidized.

Interestingly, although the degree of conjugation of **4** is higher than that of **6** and **2**, evidenced by the longer λ_{max} and the higher molar absorptivity value, the oxidative potential of **4** is lower compared to that of **2** and **6**, which suggests the electron density of Fc is more influenced by the electron-inductive effect of the linkage. For compounds **2** and **6**, the electron-withdrawing property of the carbonyl causes the electron deficiency at the Fc moiety and makes it harder to be oxidized. And compound **6** containing double carbonyls has more positive Fc/Fc^+ potential compared to **3** with only one carbonyl. For compounds **3** and **5**, the electron-donating property of $-CH_2-$ increases the electron density of Fc, and the electron-donating property depends on the number of single-bonds. So Fc moiety of **5** is more susceptible to oxidation than the one in **3**.

On the other hand, due to the electron-withdrawing effect of the –NHCO– at the 4-position of the piperidine ring, the TEMPO moieties of compounds **2**–**5** are harder to be oxidized than that

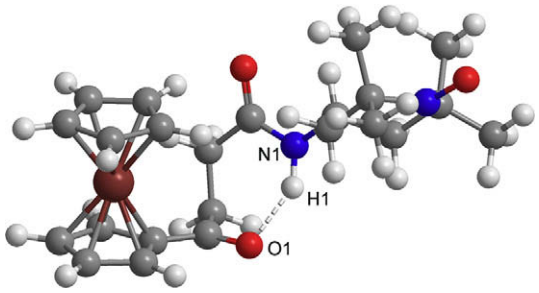

Fig. 8. DFT calculated structure of compound **6**. The calculation was carried out with the GAUSSIAN 03 program package.

of 4-NH_2-TEMPO ($E_{1/2}$ = 0.652 V). Additionally, because the electron density of TEMPO moiety is also reduced by the conjugative effect, the TEMPO/$TEMPO^+$ potential of **4** is the highest among all studied compounds. Because of the electron-donating effect of the $-CH_2-$ next to the $-NHCO-$, TEMPO/$TEMPO^+$ potentials of **3** and **5** are lower than that of **2** and **4**.

But to our surprise, compound **6** has the lowest TEMPO oxidation potential of 0.643 V among the five compounds, which may be against our speculation that the electron-withdrawing effect of the two carbonyls would raise the TEMPO/$TEMPO^+$ potential of **6**. The geometric structure analysis should help to explain it. But all efforts to obtain X-ray quality single crystal of **6** were unsuccessful. So we studied its geometric structure by molecular simulation. As shown in Fig. 8, the DFT(UB3LYP)/3-21G calculation of **6** predicted a stable conformation with an intra-molecular hydrogen bond (N1–H1···O1), which is by 4.187 kcal/mol more stable than other conformation without intra-molecular non-covalent interaction. The IR spectrum of compound **6** in CCl_4 solution showing the hydrogen-bonded NH peak at 3360 cm^{-1} (υN–H bonded), which lacks any concentration dependence (3–30 mmol/L), also indicated the intra-molecular hydrogen bonding [33,34]. Consequently, a plausible explanation for the lower TEMPO/$TEMPO^+$ potential of **6** is that the electron-withdrawing property of the carbonyl (C1=O2) is partially offset by the intra-molecular hydrogen bonds which make the TEMPO moiety of **6** easier to be oxidized, compared to **2**–**5,** as well as 4-amino-TEMPO [35].

From the electrochemistry parameters and *in vitro* ROS scavenging IC_{50} values, we found the order of antioxidative activities of the five compounds is perfectly in accordance with their first oxidation (Fc/Fc^+) potentials. The accordance clearly indicates that the Fc moiety plays a principal role in the scavenging ROS, and the antioxidative activity coincides with the ease of the oxidation of Fc moiety, i.e. the more negative the Fc/Fc^+ potential, the stronger ROS scavenging activity. From these results, we can draw a conclusion that increasing the single-bond number or reducing the carbonyl number in the linkage could decrease the Fc/Fc^+ potential effectively and improve the antioxidative activity effectively.

3. Conclusions

The present research reports the synthesis, characterization and single crystal structures of a series of novel ferrocenyl nitroxide radicals **3**–**6**. Among these compounds, **3** and **5** exhibit high *in vitro* scavenging ROS activities in low concentration. Comparative study of ROS scavenging activities, electrochemistry and UV/Vis spectra also shows that the linkage bridging Fc and cyclic nitroxide moieties is able to influence the redox property of Fc moiety and the antioxidative activity of compound dramatically. Based on this study, we speculated that decreasing the Fc/Fc^+ potential via increasing the single-bond number or reducing the carbonyl number in the linkage, is an efficient way to improve the antioxidative activity, which would guide us to develop a strategy of designing and synthesizing new functional McNOs with preferable antioxidative ability, as well as other biological activities.

4. Experimental

4.1. General

4-Amino-TEMPO radical (97%), $LiClO_4$ and luminal were bought from Sigma–Aldrich Inc. Ferrocene, formylferrocene and acetylferrocene were bought from MaoJi Fine Chemicals Co. Ltd. Ascorbate, pyrogallol, phenanthroline and other reagents were bought from Sinopharm Chemical Reagent Co. Ltd. All the reagents used in the experiments were of AR without further purification. Melting points were determined by an X-5 micro-melting point apparatus. EI-MS spectra were obtained on a Micromass GCT TOF GC/MS Spectrometer. Elemental analysis was realized with an elemental vario EL III analyzer. IR spectra were measured on Nicollet AVATAR360 FT-IR spectrophotometer. The UV/Vis spectra were recorded on a UNICO UV-2102 PC spectrophotometer. EPR measurements were performed at X-band, 9.85 GHZ, using a Bruker EMX EPR spectrometer and the measurements of *g*-factors of the compounds were carried out with a standard g-marker valued 1.9800 provided by Bruker Company. And because either ^1H NMR or ^{13}C NMR spectra was broadened by the free radical electron spin and did limited help to characterize the compounds, the NMR data were not given.

4.2. Preparation of ferrocenyl carboxylic acids

Ferroceneacetic acid, *trans*-ferrocenylacrylic acid, β-ferrocenylpropionic acid and β-ferrocenoylpropionic acid were respectively prepared following the procedure reported by literatures [10–15], and purified by recrystallization in methanol. The yields were 51%, 82%, 91% and 71%, respectively.

4.3. General procedure for the preparation of compounds ***3***–***6***

Appropriate ferrocenyl carboxylic acid (2 mmo1) was dissolved in dichloromethane (30 mL). HOBt (270 mg, 2 mmol) and DCC (412 mg, 2 mmol) were added to the solution sequentially and stirred for 0.5 h. Then 4-amino-TEMPO (342 mg, 2 mmol) was added and stirred for another 12 h [16]. The mixture was concentrated by removing dichloromethane under reduced pressure and poured into ethyl acetate (200 mL). After being placed in a refrigerator overnight, the mixture was filtered and removed of solvent under reduced pressure. The residue was purified by column chromatography on silica-gel column using petroleum ether (60–90 °C)/ethyl acetate as eluent. Yields and characterizations of compounds **3**–**6** are given below.

*4.3.1. 2-Ferrocenyl-N-(oxyl-2,2,6,6-tetramethylpiperidin-4-yl)acetamide radical (**3**)*

Yield: 54%. Yellow solid, m.p. 117–119 °C. IR (KBr υ/cm^{-1}): 3259 (υ), 3071 (υ), 2976 (υ), 1636 (υ), 1551 (δ), 1461 (δ), 1333 (υ). MS-EI: *m*/*z* 397 $[M]^+$. Anal. Calc. for $C_{21}H_{28}FeNO_3$: C, 63.48; H, 7.36; N, 7.05. Found: C, 63.36; H, 7.72; N, 6.90%. EPR: α_N in CH_2Cl_2: 15.74 G; *g* value = 2.0071.

*4.3.2. Trans-3-ferrocenyl-N-(oxyl-2,2,6,6-tetramethylpiperidin-4-yl)acrylamide radical (**4**)*

Yield: 76%. Red prisms, m.p. 123–124 °C. IR (KBr υ/cm^{-1}): 3260 (υ), 3082 (υ), 2972 (υ), 1653 (υ), 1545 (δ), 1461 (δ), 1363 (υ). MS-EI: *m*/*z* 409 $[M]^+$. Anal. Calc. for $C_{22}H_{29}FeN_2O_2$: C, 64.55; H, 7.14; N,

6.84. Found: C, 64.23; H, 7.55; N, 6.51%. EPR:α_N in CH_2Cl_2: 15.74 G; *g* value = 2.0070.

4.3.3. 3-Ferrocenyl-N-(oxyl-2,2,6,6-tetramethylpiperidin-4-yl)propanamide radical (**5**)

Yield: 65%. Yellow prisms, m.p. 82–85 °C; IR (KBr υ/cm^{-1}): 3318 (υ), 3093 (υ), 1645 (υ), 1546 (δ), 1459 (δ), 1359 (υ); MS-EI: *m*/*z* 411 [M]$^+$. Anal. Calc. for $C_{22}H_{31}FeN_2O_2$: C, 64.24; H, 7.60; N, 6.81. Found: C, 64.56; H, 7.76; N, 6.42%. EPR:α_N in CH_2Cl_2: 15.75 G; *g* value = 2.0074.

4.3.4. 3-Ferrocenoyl-N-(oxyl-2,2,6,6-tetramethylpiperidin-4-yl)propanamide radical (**6**)

Yield: 70%. Red prisms, m.p. 87–90 °C. IR (KBr υ/cm^{-1}): 3341 (υ), 3084 (υ), 2969 (υ), 1647 (υ), 1640 (υ), 1544 (δ), 1455 (δ), 1363 (υ). MS-EI: *m*/*z* 439 [M]$^+$; Anal. Calc. for $C_{23}H_{31}FeN_2O_3$: C, 62.88; H, 7.11; N, 6.38. Found: C, 63.09; H, 7.18; N, 6.03%. EPR:α_N in CH_2Cl_2: 15.75 G; *g* value = 2.0074.

4.4. X-ray crystallography

Suitable single crystals of compounds **4** and **5** were grown from slow diffusion of petroleum ether into ethyl acetate solution at room temperature. The single-crystal X-ray diffraction studies were carried out on a Bruker SMART APEX CCD diffractometer with a Mo Kα (λ = 0.7103) sealed tube following the standard procedures at room temperature. Data collection and cell refinement were carried out with the Bruker SMART. The Bruker SHELXTL was used for Data reductions. The crystal structures were solved and refined using the SHELXL97 [36]. All non-hydrogen atoms were refined anisotropically, while the hydrogen atoms were introduced at calculated positions and refined riding on their carrier atoms. Crystallographic data and refinement details are listed in Table 3. Selected bond lengths and angels are given in the captions of Figs. 1 and 3.

Table 3
Crystallographic data for **4** and **5**.

Compound	**4**	**5**
Formula	$C_{22}H_{29}FeN_2O_2$	$C_{22}H_{31}FeN_2O_2$
Formula weight	409.16	411.34
Crystal system	Monoclinic	Monoclinic
Space group	$P2_1/c$	$P2_1/c$
a (Å)	30.862 (5)	18.843 (2)
b (Å)	13.297 (2)	11.2880 (13)
c (Å)	10.6917 (18)	10.1316 (11)
β (°)	99.447	101.837 (2)
μ (mm^{-1})	0.72	0.73
V (Å^3)	4327.9 (12)	2109.2 (4)
Z	8	4
D_{calc} (Mg m^{-3})	1.312	1.295
F(0 0 0)	1816	876
Crystal color/morphology	Red, prismatic	Yellow, prismatic
Crystal size(mm)	0.37 × 0.11 × 0.04	0.41 × 0.30 × 0.22
θ Range for data collection(°)	5.3–37.0	5.6–47.8
Cell parameters from reflections	529	253
Index range	$-37 \le h \le 36$, $-13 \le k \le 16$	$-24 \le h \le 21$, $-14 \le k \le 8$
Maximum and minimum transmission	0.708 and 1.000	0.708 and 1.000
Reflection collected/unique	8041	4597
Reflection observed [$I \ge \sigma(I)$]	3953	3117
R_{int}	0.143	0.112
$R[F^2 > 2\sigma(F^2)]$	0.084	0.046
$wR(F^2)$	0.236	0.133
$\Delta\rho$ (e Å^{-3})	0.890, −0.420	0.330, −0.390

4.5. Superoxide anion scavenging activity assay

The $O_2^{\cdot-}$ scavenging activities of **2**–**6** were determined by pyrogallol-luminol system CL on a BPCL Ultra-weak luminescence analyzer [23,24]. Ten milliliter of sample DMSO solution at different concentration and 50 μL of pyrogallol (0.625 mmol/L) were mixed in a glass test tube. Then 0.94 mL of a mixture containing luminal (0.05 mol/L) and carbonate buffer (pH 10.2) was added to initiate the chemiluminescence reaction. The emission light intensity was recorded every second and accumulated continuously for 100 s. The control test was performed following the same procedure except the sample solution is replaced by DMSO, and the background test was detected with only luminol and buffer. Each test was repeated at least three times. The scavenging activity for $O_2^{\cdot-}$ was calculated as:

$$\text{Scavenging activity} = \frac{(CL_{control} - CL_0) - (CL_{sample} - CL_0)}{CL_{control} - CL_0} \times 100\%$$

where $CL_{control}$ was the relative luminescent intensity of the control group, CL_0 was the relative luminescent intensity of the background group and CL_{sample} was the relative luminescent intensity of the experimental group.

4.6. Hydroxyl radical scavenging activity assay

The (·OH) scavenging activities of **2**–**6** were measured by $CuSO_4$–Phenanthroline–ascorbate–H_2O_2 system CL [22]. Ten milliliter of sample DMSO solution at different concentration, 50 μL of a 1 mmol/L $CuSO_4$ solution, 50 μL of a 1 mmol/L 1,10-phenanthroline solution, 740 μL of a 0.05 mol/L borate buffer (pH 9.0) and 100 μL of a 1 mmol/L ascorbate solution were mixed in a glass test tube. Then 50 μL of a 0.15% H_2O_2 solution was added to initiate the chemiluminescence reaction. The emission light intensity was recorded every second and accumulated continuously for 70 s. The control test was performed following the same procedure in the mixture except the sample solution is replaced by DMSO, and the background test was detected with only 1,10-phenanthroline and buffer. Each test was repeated at least three times. The scavenging activity for (·OH) was calculated by the formula mentioned above.

4.7. Electroanalytical procedures

Cyclic voltammetric measurements of **2**–**6** (0.5 mmol/L) were carried out in dry acetonitrile solution containing 0.1 mol/L lithium perchlorate as supporting electrolyte, at different sweep rates from 0.02 to 0.80 Vs^{-1}, with CHI440A Electrochemical Analyzer controlled by personal computer. The conventional three-electrode setup was used with a platinum electrode as the working electrode, a platinum wire as the counter electrode, and a saturated calomel electrode (SCE) as the reference electrode.

Acknowledgements

We wish to thank Prof. Zhong Li, Prof. Yun Tang and Dr. Feng Fan of the Shanghai Key Laboratory of Chemical Biology (ECUST), who offer us much help such as molecular simulation. This work was supported by the EU Framework Programme 6 Integrated Project Novel and Improved Nanomaterials, Chemistries and Apparatus for Nano-biotechnology (NACBO) (contract No.500804), Shanghai Nano-Technology Promotion Center (SNPC) 0652nm020 and the Ministry of Science and Technology of the People's Republic of China (contract No.0424). All the calculations were performed on the supercomputer at Supercomputer Center of East China University of Science and Technology.

Appendix A. Supplementary data

CCDC 726881 and 726877 contain the supplementary crystallographic data for compounds **4** and **5**. These data can be obtained free of charge from The Cambridge Crystallographic Data Centre via www.ccdc.cam.ac.uk/data_request/cif.

Supplementary data associated with this article can be found, in the online version, at doi:10.1016/j.jorganchem.2009.08.012.

References

[1] A.R. Forrester, S.P. Hepburn, R.S. Dunlop, H.H. Mills, J. Chem. Soc., D: Chem. Commun. 1969 (1969) 698–699.
[2] B. Nickel, A. Rassat, Tetrahedron Lett. 21 (1980) 2409–2412.
[3] Z.V. Todres, D.S. Ermekov, R.D. Rakhimov, V.V. Zhiltsov, V.M. Kazakova, Metalloorg. Khim. 5 (1992) 1207–1210.
[4] O. Jurgens, J. Vidal-gancedo, K. Wurst, C. Sporer, K. Worm, P. Jaitner, J. Veciana, Mol. Cryst. Liq. Cryst. Sci. Technol. Sect. A 306 (1997) 249–256.
[5] V.I. Ovcharenko, A.V. Podoplelov, Metalloorg. Khim. 2 (1989) 1136–1141.
[6] O. Juergens, J. Vidal-gancedo, C. Rovira, K. Wurst, C. Sporer, B. Bildstein, H. Schottenberger, P. Jaitner, J. Veciana, Inorg. Chem. 37 (1998) 4547–4558.
[7] Y. Wu, L.D. Miao, H.H. Yuan, S.H. Zuo, C.M. Ding, M.B. Lan, Chem. Lett. 35 (2006) 794–795.
[8] Y. Wu, W. Tang, C.L. Li, J.W. Liu, L.D. Miao, J. Han, M.B. Lan, Pharmazie 61 (2006) 1028–1033.
[9] M.B. Lan, Y. Wu, H.H. Yuan, CN Patent 1709874 7, 2005.
[10] S.H. Stephan, Angew. Chem. 109 (1997) 2569–2572.
[11] D.D. Gerald, Euro. J. Org. Chem. 2003 (2003) 3167–3172.
[12] G.D. Broadhead, J.M. Osgerby, J. Chem. Soc. 2 (1958) 650–656.
[13] C. Mario, H.B. Antonija, A. Nagl, M. Juki, V. Rapi, Struct. Chem. 14 (2003) 289–293.
[14] M. Rosenblum, A.K. Banerjee, N. Danieli, R.W. Fish, V. Schlatter, J. Am. Chem. Soc. 85 (1963) 316–324.
[15] L. Kenneth, J. Rinehart, R.J.R. Cursu, J.S.E. Phillip, J. Am. Chem. Soc. 79 (1957) 3420–3424.
[16] J. Wang, F.L. Tang, Chin. Chem. Lett. 13 (2002) 1055–1056.
[17] A.P. Krukonis, J. Silverman, N.F. Yannoni, Acta Cryst. B 28 (1972) 987.
[18] E. Damiani, C. Belaid, P. Carloni, L. Greci, Free Radical Res. 37 (2003) 731–741.
[19] A.M. Samuni, Y. Barenholz, Free Radical Biol. Med. 34 (2003) 177–185.
[20] G. Mugesh, A. Panda, H.B. Singh, N.S. Punekar, R.J. Butcher, Chem. Commun. 1998 (1998) 2227–2228.
[21] B.P. Soule, F. Hyodo, K. Matsumoto, N.L. Simone, J.A. Cook, M.C. Krishna, J.B. Mitchell, Free Radical Biol. Med. 42 (2007) 1632–1650.
[22] T. Sun, Z. Xu, Bioorg. Med. Chem. Lett. 16 (2006) 3731–3734.
[23] P. Yu, C. Hu, E.J. Meehan, L. Chen, Chem. Biodivers. 4 (2007) 508.
[24] Y. Wenli, Z. Yaping, BBA-General Subjects 1725 (2005) 30–34.
[25] T.M. Triantis, E. Yannakopoulou, A. Nikokavoura, D. Dimotikali, K. Papadopoulos, Anal. Chim. Acta 591 (2007) 106–111.
[26] Y. Wu, C.M. Ding, L. Miao, H.H. Yuan, M.B. Lan, Chin. Pharm. J. 42 (2007) 1380–1383.
[27] H.L. Zhao, J.H. Wu, X.J. Meng, S.H. Zuo, W.T. Wang, H.H. Yuan, M.B. Lan, J. Heterocyclic Chem. 45 (2008) 371–376.
[28] J.A. Harrison, Z. Khan, J. Electroanal. Chem. 28 (1970) 131–138.
[29] N.F. Blom, E.W. Neuse, H.G. Thomas, Transition. Met. Chem. 12 (1987) 301–306.
[30] S. Manda, I. Nakanishi, K. Ohkubo, H. Yakumaru, K. Matsumoto, T. Ozawa, N. Ikota, S. Fukuzumi, K. Anzai, Org. Biomol. Chem. 5 (2007) 3951–3955.
[31] A.C. Herath, J.Y. Becker, Electrochim. Acta 53 (2008) 4324–4330.
[32] P. Debroy, M. Banerjee, M. Prasad, S.P. Moulik, S. Roy, Org. Lett. 7 (2005) 403–406.
[33] C.P. Rao, R. Nagaraj, C.N. Rao, P. Balaram, FEBS Lett. 100 (1979) 244–248.
[34] Z.D.R. Margeta, M. Vinkovi, Z. Tefani, P.B. Koji, M.K. Mlinari, M. Ini, J. Mol. Struct. 876 (2008) 218–224.
[35] Y.F. Yuan, L.Y. Zhang, J.P. Cheng, J.T. Wang, Transition Met. Chem. 22 (1997) 281–283.
[36] G.M. Sheldrick, SHELX Suite of Programs for Crystal Structure Solution and Refinement[Z], 1997.